Lab on a Chip

Micromixer driven by bubble-induced acoustic microstreaming for multi-ink 3D bioprinting

Journal:	*Lab on a Chip*
Manuscript ID	LC-ART-06-2024-000552.R1
Article Type:	Paper
Date Submitted by the Author:	19-Aug-2024
Complete List of Authors:	Hidaka, Mitsuyuki; Osaka University Graduate School of Engineering Science School of Engineering Science Kojima, Masaru; Osaka University Graduate School of Engineering Science School of Engineering Science Sakai, Shinji; Osaka University, Engineering Science; Osaka University, Engineering Science

ARTICLE

Micromixer driven by bubble-induced acoustic microstreaming for multi-ink 3D bioprinting

Received 00th January 20xx,
Accepted 00th January 20xx

DOI: 10.1039/x0xx00000x

Mitsuyuki HIDAKA[a], Masaru KOJIMA [a], and Shinji SAKAI[a]*

Recently, the 3D printing of cell-laden hydrogel structures, known as bioprinting, has received increasing attention owing to advances in tissue engineering and drug screening. However, a micromixing technology that efficiently mixes viscous bioinks under mild conditions is needed. Therefore, this study presents a novel method for achieving homogeneous mixing of multiple inks in 3D bioprinting through acoustic stimulation. This technique involves generating an acoustic microstream through bubble oscillations inside a 3D bioprinting nozzle. We determined the optimal hole design for trapping a bubble, hole arrangement, and voltage for efficient mixing, resulting in a four-fold increase in mixing efficiency compared to a single bubble arrangement. Subsequently, we propose a nozzle design for efficient mixing during bioprinting. The proposed nozzle design enabled the successful printing of line structures with a uniform mixture of different viscous bioinks, achieving a mixing efficiency of over 80% for mixing 0.5–1.0 wt% sodium alginate aqueous solutions. Additionally, acoustic stimulation had no adverse effects on cell viability, maintaining a high cell viability of 88% after extrusion. This study presents the first use of a bubble micromixer in 3D bioprinting, demonstrating gentle yet effective multi-ink mixing. We believe this approach will broaden 3D printing applications, particularly for constructing functional structures in 3D bioprinting.

Introduction

Three-dimensional (3D) printing is a transformative fabrication technology that enables the cost-effective construction of 3D structures from digital data.[1,2] Recently, the 3D printing of cell-laden hydrogel structures, known as bioprinting, has received increasing attention owing to advances in tissue engineering and drug screening.[3–5] To date, several printing techniques, including extrusion-, vat-polymerisation-, and inkjet-based bioprinting, have been explored to meet these demands.[6–8] Among these, extrusion-based bioprinting, in which a material is extruded from an extruder, is the most popular owing to its simplicity, versatility, and ability to print a wide range of bioinks.[9] Especially, this printing technique has the capability to use inks of varying viscosities and print large-scale 3D structures (cm^3 scale) compared to other techniques[9].

Further development of extrusion-based bioprinting requires advancements in two key aspects: the development of bioinks and the improvement of print fidelity and functionality of the resulting cell-laden structures. The ideal bioinks for extrusion-based bioprinting should be biocompatible and degradable, rapidly solidify, and have rheological properties that maintain structural integrity post-extrusion without decreasing cell viability due to shear stress during printing.[10,11] Bioinks with shear-thinning properties are particularly desirable for extrusion-based bioprinting. Bioinks comprising alginate, hyaluronic acid, and gelatin exhibit these properties and are frequently used.[7,8] Additionally, various printing techniques, such as multi-ink printing and printing in support baths, have been developed to improve the print fidelity and functionality of the resulting cell-laden structures.[12,13] Multi-ink mixing is particularly significant because it controls the cell density and crosslinking reaction of bioinks, determining the stiffness and functionality of the printed structure.[2,12] For instance, cell growth and differentiation are hugely affected by the stiffness of the scaffold[13, 14]. Hence, there is a need for technology that can control the ink composition depending on the type of cell to facilitate complex structures mimicking native tissue consisting of several types of cells. Typical extrusion-based bioprinting involves the extrusion of bioinks under laminar flow conditions,[15,16] where the bioinks are not easily mixed without external stimulation. Therefore, incorporating effective mixing techniques into extrusion-based 3D bioprinting under such conditions is critical to achieve high-quality printing.

Mixing techniques can be categorised into passive and active mixing. Passive mixing occurs without the application of external forces. Some methods use a zigzag path or baffles attached to the nozzles to enhance mixing efficiency.[17,18] Although passive mixing operates under mild conditions, it generally requires a long mixing time, a large mixing chamber volume, and a limited ability to mix highly viscous materials.[16] By contrast, active mixing uses external forces, such as heat and physical stirring, to mix various viscous materials.[19,20] While it can mix viscous materials quickly, active mixing can generate

[a] Division of Chemical Engineering, Department of Materials Engineering Science, Graduate School of Engineering Science, Osaka University, 1-3 Machikaneyama-cho, Toyonaka, Osaka, Email: sakai@cheng.es.osaka-u.ac.jp

† Supplementary Information available: [details of any supplementary information available should be included here]. See DOI: 10.1039/x0xx00000x

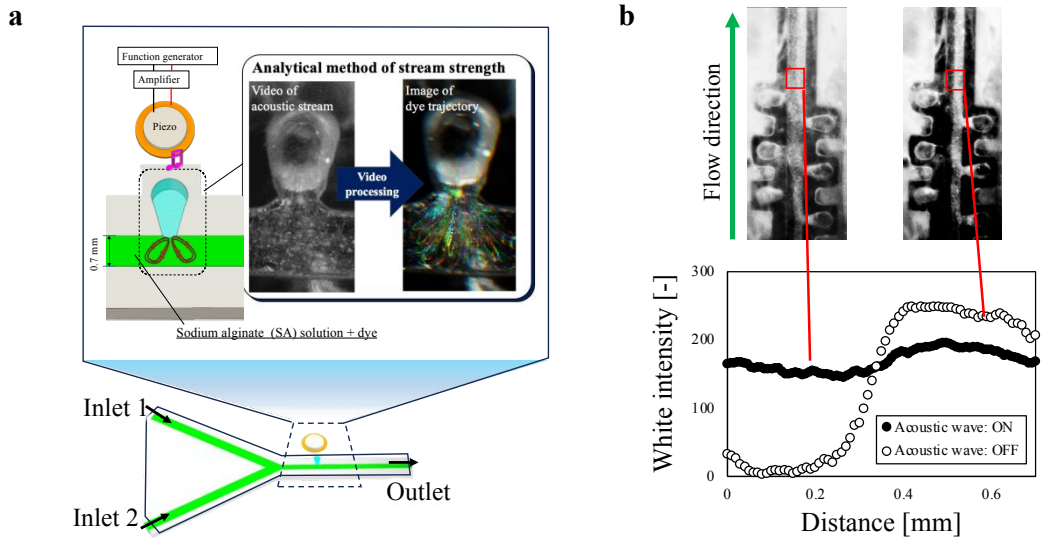

Fig. 1 (a) Overall view of observation system and acoustic nozzle. (b) White intensity profiles of outlets in from photos.

high shear stress that can damage cells.[21] Integrating mechanical mixers into microfluidic devices is challenging, necessitating the development of a micromixing technology that can efficiently mix viscous bioinks under mild conditions.

Acoustic stimulation is a promising technique for achieving gentle yet effective mixing.[22,23] It is a non-invasive and gentle method for biomaterials[24,25] used in bio-related applications such as cell patterning and separation.[24,26] Bubble-induced acoustic micromixers effectively stimulate material mixing.[22,23,25] In this technique, acoustic waves vibrate the bubbles trapped in the path of the mixer, resulting in microstreams through pressure fluctuations that effectively mix the materials. This process typically occurs at room temperature and can be applied to a wide range of materials,[27,28] making it valuable for biomedical applications and chemical synthesis.[25,29,30]

In this study, we applied a bubble-induced acoustic micromixer for bioink mixing in extrusion-based 3D bioprinting. Initially, we investigated the hole design for trapping bubbles, hole arrangement, and operating conditions for efficient mixing using sodium alginate (SA) aqueous solutions as a bioink. SA is known for its biocompatibility and shear-thinning properties, and it can be gelled instantaneously upon contact with a solution containing calcium ions, making it a suitable bioink for cell-laden hydrogels in bioprinting.[31,32] After determining the optimal conditions, we proposed an acoustic nozzle with high mixing efficiency and integrated it into the 3D printing process. The developed nozzle could mix viscous SA inks in a smaller volume mixing chamber than typical passive and active mixers. Furthermore, we assessed the effect of acoustic stimulation on cell viability inside the nozzle. The nozzle did not hugely affect the cell viability. Finally, the versatility of the nozzle was tested using a photocurable chitosan ink in addition to SA. This is the first study to apply an acoustic micromixer to 3D printing technology (bioprinting). We believe this technological advancement will significantly broaden 3D printing applications, particularly bioprinting.

Materials & methods

Materials

SA (molecular weight: 70 kDa; I-1G) was purchased from Kimica (Tokyo, Japan). Chitosan (Chitosan LL, deacetylation: 80%, weight average molecular weight: 50–100 kDa) was purchased from Yaizu Suisankagaku Industry (Shizuoka, Japan). Lactobionic acid, N,N,N′,N′-tetramethylethylenediamine (TEMED), and sodium persulfate (SPS) were purchased from Fujifilm-Wako Chemicals (Tokyo, Japan). $Ru(bpy)_3 \cdot Cl_2 \cdot 6H_2O$, 1-ethyl-3-(3-dimethylaminopropyl) carbodiimide hydrochloride (EDC·HCl), and 3-(4-hydroxyphenyl) propionic acid (HPP) were purchased from Sigma-Aldrich (St. Louis, Missouri, USA), Peptide Institute (Osaka, Japan), and Tokyo Chemical Industry (Tokyo, Japan), respectively. Mouse fibroblast 10T1/2 cells were purchased from Riken Cell Bank (Ibaraki, Japan). The cells were cultured in Dulbecco's modified Eagle's medium (DMEM; Nissui, Tokyo, Japan) with 10 vol% fetal bovine serum in a 5% CO_2 incubator. The phenol derivative of chitosan (Ch-Ph) was prepared based on the literature by conjugating chitosan and HPP using EDC·HCl and TEMED.[33,34]

Nozzle preparation

The acoustic nozzle shown in Fig. 1(a) was designed using computer-aided design (CAD) software (Fusion360, Autodesk, California, USA). The nozzle was fabricated from clear photocurable plastic resin (NOVA3D High Transparency UV Resin, Shenzhen Nova Intelligent Technology Co., Shenzhen, China) using a vat-polymerisation-based 3D printer (Anycubic Photon Ultra, Shenzhen Anycubic Technology, Shenzhen, China). The nozzle depth and diameter were 0.7 mm, featuring two inlets, one outlet, and holes with diameters ranging from 0.30 to 0.87 mm to trap bubbles in the nozzle path. The hole design used to trap bubbles was based on literature to achieve efficient mixing.[35] The fabricated nozzle was then attached to a

glass plate (C040501; Matsunami Glass, Ind. Ltd., Osaka, Japan) with a photocurable, clear plastic resin. 22-gauge needles were attached to the inlets and outlets with the resin. A piezoelectric transducer was attached to a glass slide along the side of the nozzle using silicone adhesive (Shin-Etsu Chemical Co., Tokyo, Japan). The nozzle was coated with the adhesive to prevent the ink leaking (Fig. S1).

Experimental setup

A syringe pump (KDS 220, KD Scientific Inc., Massachusetts, USA) was used to extrude SA solutions containing and not containing 0.1 wt% green fluorescent particles into the acoustic nozzle. The extruded SA solutions were mixed using the nozzle via acoustic stimulation. The transducer was driven by a function generator (Fujian Lilliput Optoelectronics Technology Co., Ltd., Fujian, China), and the voltage was amplified using an amplifier (HJPZ-0.15P×3, Matsusada Precision Inc., Shiga, Japan) (Fig. 1(a)).

Mixing behaviour was observed under a stereoscopic microscope (SZ-CTV, Olympus, Tokyo, Japan). A commercially available 3D printing system (FLSUN-QQ-S, Zhengzhou Chaokuo 114 Electronic Technology Co., Henan, China) was used for 3D printing.[33] Blue light was used as a light source for clear observation. The overall experimental setup is shown in Fig. S1. The SA solutions were extruded from the syringe pump through the acoustic nozzle, and the line structure of the SA solution was printed using a 3D printer. A 1.0 wt% calcium chloride aqueous solution was added for hydrogelation. In addition, the versatility of the acoustic mixing system was evaluated using a visible-light-curable chitosan-phenol (Ch-Ph) bioink. SPS and $Ru(bpy)_3$ were added to the Ch-Ph aqueous solution at 2.0 mM and 1.0 mM, respectively. The solution was exposed to visible blue light (λ = 450 nm, 0.14 W/m^2) during the printing process for hydrogelation. The printed line structures were observed under the stereoscopic microscope.

Strength evaluation of bubble-induced acoustic microstream

The effects of hole design, SA concentration (0.5–2.0 wt%), and voltage applied to the piezoelectric transducer were investigated. The SA solution containing 0.1 wt% fluorescent particles was filled in the nozzle. An acoustic wave was applied to the nozzle at 5–60 V for 6 s, and the white and black video was captured (Video S. 1). From the video, the trajectory of the particles was obtained using a plugin[36] of the image-processing software, ImageJ (version 1.53a, NIH, Maryland, USA).

Mixing efficiency evaluation of bubble-induced acoustic microstream

The mixing efficiency of the SA solution by the bubble-induced acoustic microstream was investigated for 0.5–2.0 wt% SA solutions. Solutions with and without fluorescent particles flowed from two inlets. The flow of the aqueous solutions under acoustic stimulation was recorded, and the white intensity from the fluorescent particles in the solution was analysed at the end of the mixing chamber (shown as a red square in Fig. 1(b)). The grey intensity profile of the area was obtained. The degree of mixing caused by the acoustic waves was numerically evaluated by calculating the mixing index (MI), defined as follows based on the literature:[37]

$$\mathrm{MI} = 1 - \frac{\sqrt{\frac{1}{N}\sum_i^N (I_i - \bar{I})}}{\bar{I}} \quad (1)$$

where I_i denotes the white-point intensity of the mixing chamber shown as a red square in Fig 1(b)), $\bar{I}$ represents its average intensity, and N indicates the number of sampling points. MI was calculated from the white light intensity data of the solution at the outlet (Fig. 1(b)). When this value is close to 1, homogeneous mixing occurs.

Effect of acoustic mixing on cell viability

DMEM containing 0.5 wt% SA and either containing or not containing 1.5 × 10^4 cells/mL 10T1/2 cells was extruded from the nozzle at 0.9 mm/s from the inlets into a sample tube under acoustic stimulation at 45 V, 3.0 kHz. The total flow rate was 1.8 mm/s. The cells in the solutions flowing out of the nozzle were stained with trypan blue, and cell viability was calculated by counting dead and live cells.[38] For comparison, cell viability was

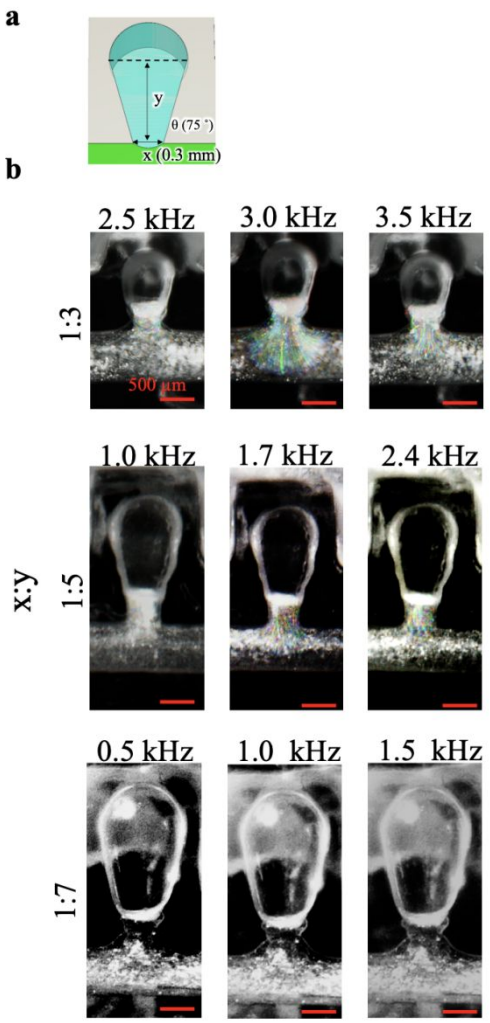

Fig. 2 (a) Design of the hole for trapping air bubbles. (b) Effect of bubble size on bubble-induced acoustic microstreaming.

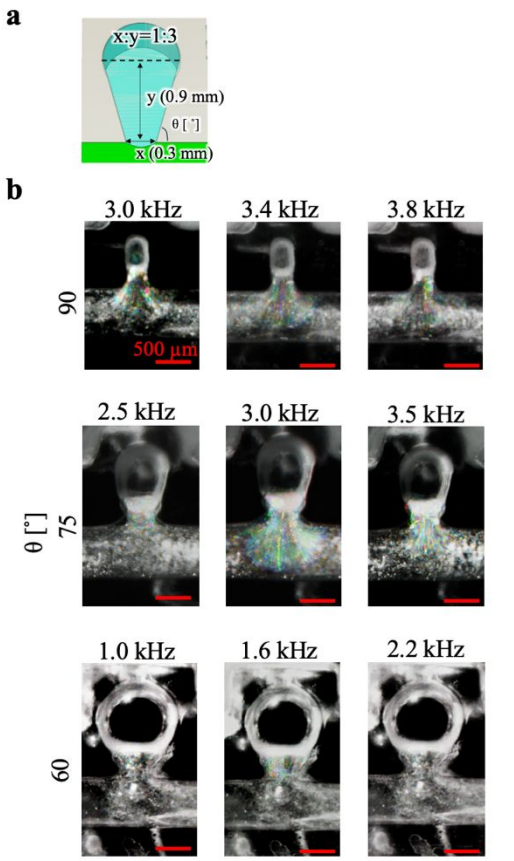

Fig. 3 (a) Design of the hole for trapping air bubbles. (b) Effect of the hole angle on bubble-induced acoustic microstreaming.

also measured in the extruded solution without acoustic stimulation.

Result & discussion

Effect of hole size

First, the effect of hole size on the bubble-induced acoustic microstream was evaluated using a 0.5 wt% SA solution. We expected the hole design to be an important factor for creating a prominent microstream. Each prepared nozzle contained holes to trap air bubbles of different sizes (Fig. 2(a)). The bubble was stable for at least 15 hours as shown in Fig. S2. The minimum hole diameter was 0.3 mm at a 75˚ angle against the nozzle wall. The nozzle was filled with SA solution containing fluorescent particles, and an acoustic wave was applied at 15 V. A prominent stream was observed in the nozzle with a 1:3 aspect ratio at 3.0 kHz (Fig. 2(b)). The vibration strength of the bubble oscillation increased with frequency until it reached the natural frequency.[39] When a higher frequency was applied to the bubble, vibration did not occur because the vibration phases of the bubble and liquid became identical. The results showed that a typical phenomenon of bubble oscillation occurred in the nozzle and that hole design was an important factor for efficient mixing [25, 39].

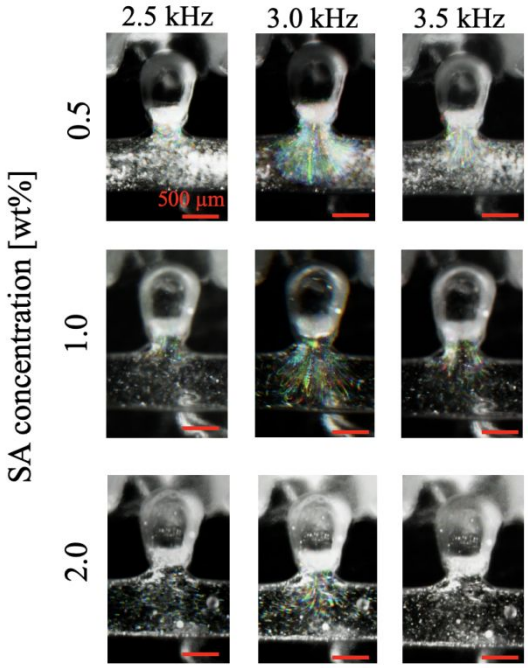

Fig. 4 Effect of SA concentration on bubble-induced acoustic microstream.

Effect of hole angle against the wall

We also expected the hole angle against the channel wall to be an important factor in the microstream. The effect of the hole angle relative to the wall on the bubble-induced acoustic microstream was investigated using three types of nozzles with different hole angles (Fig. 3(a)). As shown in Fig. 3(b), prominent streams were observed at 3.4 kHz, 3.0 kHz, and 1.6 kHz at hole angles of 90°, 75°, and 60˚, respectively. The most prominent stream was observed in the nozzle with a hole angle of 75° against the wall. Theoretically, a more prominent stream should be observed at a higher frequency when higher energy is applied to the bubble. Although the highest frequency that caused a prominent stream was 3.4 kHz at the nozzle with a 90˚-hole angle among the prepared nozzles, the bubble did not face the channel directly, resulting in a weak stream. Based on these results, we determined that the appropriate angle was 75˚.

Effect of SA concentration

Furthermore, based on the above results, we investigated the effect of SA concentration on bubble-induced acoustic

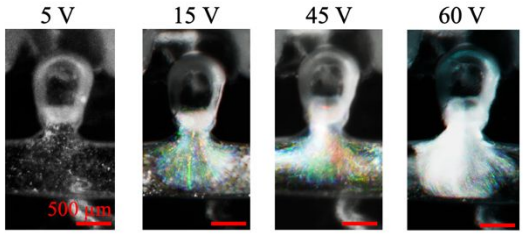

Fig.5 The effect of voltage on bubble-induced acoustic microstream.

microstreams using a nozzle with a hole having a 1:3 aspect ratio and at an angle of 75˚. The nozzle was filled with 0.5, 1.0, and 2.0 wt% SA solutions, and acoustic stimulation was applied at 15 V at different frequencies (2.5, 3.0, and 3.5 kHz). Although the strength of the stream decreased with increasing SA concentrations, a prominent stream was observed at 3.0 kHz for all concentrations (Fig. 4). Theoretically, the resonance frequency of a bubble depends on the bubble diameter and surface tension between the air bubble and solution.[27] In addition, the surface tension of an SA solution in air depends on the SA concentration.[40] However, the difference observed was only within 10 mN/m (Table S1). We suggest that the change in surface tension did not significantly affect the frequency in this concentration range and that the diameter of the air bubble was the dominant factor in this condition.

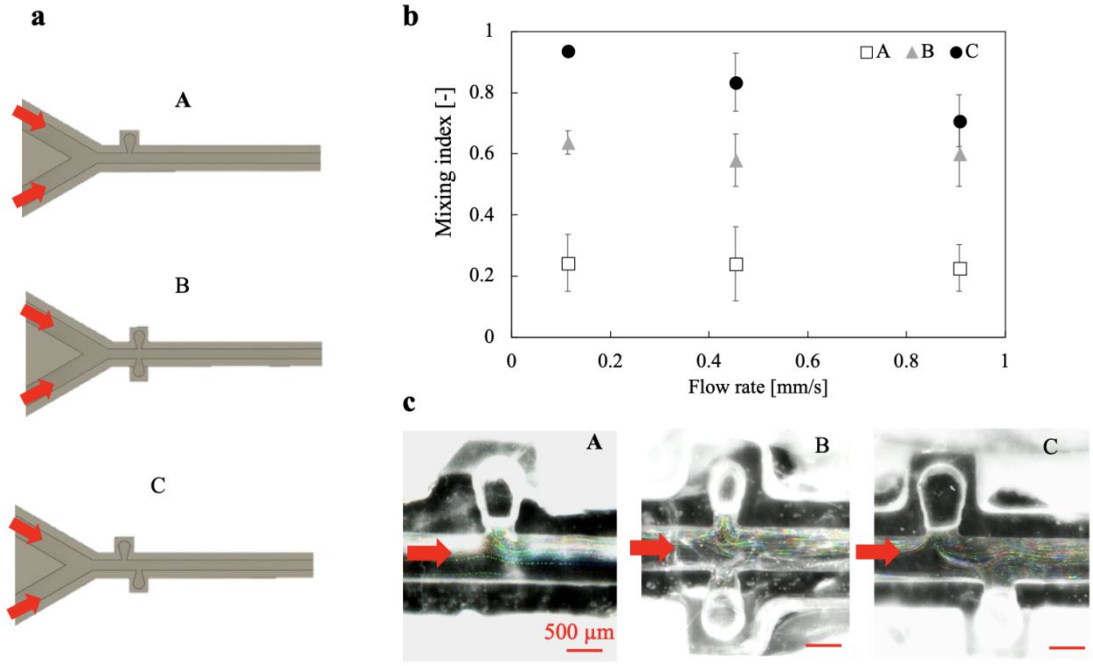

Fig. 6 (a) Nozzles with different hole arrangements. (b) Mixing indexes of nozzles at different flow rates (n = 5, Data: Mean ± SD). (c) Stream formed in each channel.

Effect of voltage on bubble-induced acoustic microstream

In addition, the effect of the voltage on the bubble-induced acoustic microstream was measured. Acoustic stimulation was applied to the nozzle at 3.0 kHz and 5–60 V. We visually confirmed that the strength of the stream was enhanced with increasing voltage (Fig. 5). The amount of energy in an acoustic wave is closely related to its frequency and amplitude, as a higher frequency or amplitude results in an acoustic wave with greater energy. An acoustic wave is formed by an electrically driven piezoelectric transducer. Thus, a higher voltage should result in a higher amplitude of the acoustic waves, leading to a more prominent stream. However, the piezoelectric transducer generating the acoustic wave broke at 60 V due to the overvoltage. Therefore, we determined that the optimal condition was 45 V and 3.0 kHz. However, a more prominent stream should be obtainable using a more durable piezoelectric transducer.

Effect of hole arrangement

After determining the appropriate hole design, the viscous solutions were mixed using a nozzle. First, a nozzle with a single bubble (Fig. 6(a), shown as A) was used to mix the 0.5 wt% SA solutions at 0.1, 0.45, and 0.9 mm/s. Efficient mixing did not occur in this nozzle at any flow rate (Fig. 6(b)(c), shown as A). These results suggest that multiple bubbles are required to mix viscous solutions. Consequently, two types of nozzles with two types of bubble arrangements were prepared, and their mixing performances were evaluated. One nozzle had two bubbles facing each other, while the other nozzle had two bubbles arranged zigzagly (Fig. 6(a), shown as B and C). The former nozzle could not mix the solutions well because the streams formed by each bubble cancelled each other out. The latter nozzle mixed the solutions with higher efficiency (Fig. 6(b)(c), shown as C) than the other nozzles (shown as A and B). The solutions released from the first bubble were efficiently incorporated into the next bubble in the nozzle, resulting in efficient mixing. This design aligns well with previous literature.[30,35] We determined that the zigzag bubble arrangement was optimal.

Effects of viscosity and flow rate on mixing

Based on the aforementioned results, we propose an acoustic nozzle for highly efficient mixing during 3D printing (Fig. 7(a)). The nozzle has six bubbles arranged in a zigzag pattern. The mixing chamber volume was 2.45 mm^3 (depth = 0.70 mm, width

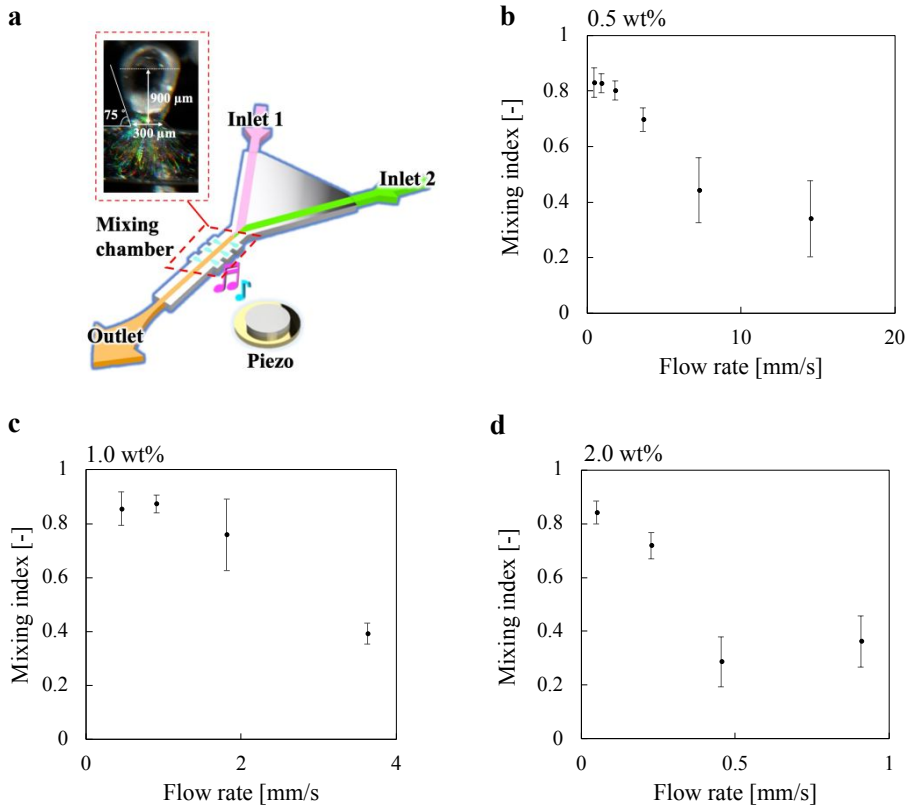

Fig. 7 (a) Proposed nozzle for mixing bioinks with high efficiency and the effect of flow rate on mixing in (b) 0.5, (c) 1.0, and (d) 2.0 wt% SA solutions (n = 5, Data: Mean ± SD).

= 0.70 mm, chamber length = 5.0 mm). We investigated the effects of viscosity and flow rate on mixing using the proposed nozzle with 0.5, 1.0, and 2.0 wt% SA solutions (Fig. 7(b)–(d)). Solutions with and without fluorescent particles flowed from the two inlets (Fig. 7(b)), and the mixing behaviour was observed as shown in Fig. 1(b). The maximum flow rates demonstrating high efficiency were up to 1.80, 0.90, and 0.05 mm/s for the 0.5, 1.0, and 2.0 wt% aqueous solutions, respectively (MI = 80 ± 3.4%, 87 ± 3.1%, 84 ± 4.2%). A video of 0.5 wt% SA solution being mixed can be seen in Video S2. These results showed that the mixing behaviour was strongly affected by the viscosity of the solution. Generally, a bioink is extruded from a nozzle at a few hundred µm/s to a few mm/s.[33,41] Therefore, the nozzle with the bubble-induced acoustic micromixer could mix 0.5 and 1.0 wt% SA solutions under bioprinting conditions. However, the nozzle did not mix the 2.0 wt% SA solution with high efficiency under the printing conditions. The viscosity data showed that the 2.0 wt% SA solution was 20 times higher than that of the 0.5 wt% SA solution, requiring significant mixing energy. The viscosity profiles of these SA solutions are shown in Fig. S3. Therefore, another nozzle design, such as a nozzle with more bubbles or baffle boards, should be considered as passive mixers for mixing more viscous solutions[42,43] or attaching a piezo with higher voltage resistance.

Mixing of different viscous SA solutions

Furthermore, we attempted to mix SA solutions with different viscosities using an acoustic nozzle. The 0.5 and 1.0 wt% SA solutions were mixed in a micromixer. The results showed that these solutions mixed well up to a flow rate of 0.90 mm/s (*MI* = 80 ± 4.7%, Fig. 8). Micromixing technology has been applied in various fields, including biomedical and chemical processes.[37,44] Passive mixing involves passively mixing solutions using the geometry of the nozzle or baffles attached to the nozzle.[18] Although materials are mixed under mild conditions, a large nozzle path volume and a long mixing time are required. In addition, mixing viscous solutions is challenging. Passive mixers

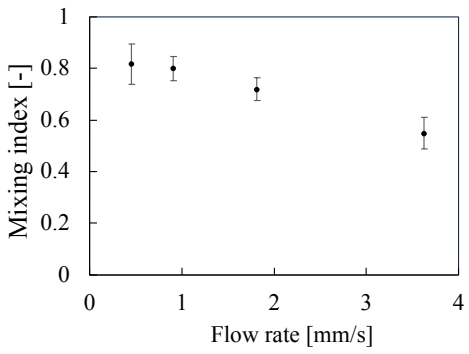

Fig. 8 Mixing performance for 0.5 and 1.0 wt% SA solutions (n = 5, Data: Mean ± SD).

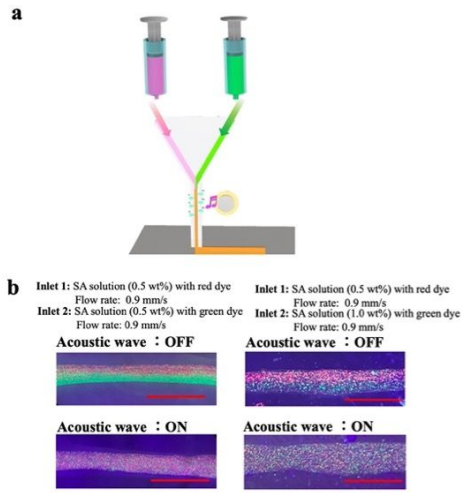

Fig. 9 (a) Schematic of the 3D printing system. (b) Printed line structures with and without acoustic wave (scale bar: 2 mm).

are currently limited to mixing low-viscosity materials, such as water and organic solvents.[1,45] Furthermore, although passive mixers have been applied to bioprinting, such as using a nozzle to mix GelMA solutions, a long path (>20 mm) and high flow rate (>375 μL/min) were required for effective mixing,[2] limiting printability. The developed nozzle in this study mixed the viscous bioinks (20–150 mPa·s) with a shorter path (<5 mm) under bioprinting conditions (65 μL/min, 1.8 mm/s). Therefore, the nozzle can mix more viscous solutions in a smaller mixing volume than passive mixers.

Conversely, active mixing involves mixing materials through external stimulations, such as heat and physical stirring.[46,47] This method can mix highly viscous materials within a short period. However, it applies high shear stress to the mixed solutions, making it unsuitable for biomedical processes. Furthermore, a technical limitation exists for attaching the mixer to a microfluidic device. For example, Ober et al. reported mixing several types of viscous materials and 3D printing by attaching a small mixer to the nozzle path.[19] However, the volume of the mixing chamber was 150 mm^3, approximately 60 times larger than that of the nozzle we developed (2.45 mm^3). Locally placing bioinks with high resolution[48] during bioprinting is necessary to build a 3D structure that imitates native tissues. The developed nozzle has the advantage of mixing a small volume of bioink compared with other active mixers.

3D printing

We demonstrated that an acoustic nozzle could mix SA bioinks under 3D bioprinting conditions. Line structures were printed using the proposed acoustic nozzle to test its effectiveness in 3D bioprinting. 0.5 wt% SA solutions with red and green fluorescent particles were used in the printing process (Fig. 9(a)). Based on the results shown in Fig. 7(a), each solution was extruded at 0.9 mm/s by syringe pumps, so the flow rate at the outlet was 1.8 mm/s, and a line structure was printed by a 3D printer. After extrusion, a 1.0 wt% calcium chloride solution was added to the structure for hydrogelation. A line structure

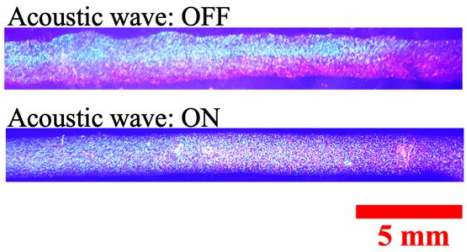

Fig. 10 Printed line structure of the 0.5 wt% SA solution (red) and 1 wt% SA solution (green) with colour gradient (scale bar: 5 mm).

coloured red and green on each side was printed when acoustic stimulation was not applied. By contrast, a line structure with mixed red and green colours was printed when acoustic stimulation was applied (Fig. 9(b)). The nozzle successfully mixed the viscous SA solutions and proved effective as a 3D bioprinting mixer.

Furthermore, 3D printing was performed using SA solutions of different viscosities. 0.5 wt% and 1.0 wt% SA solutions were used to print a line structure. Each solution was extruded at 0.45 mm/s by syringe pumps based on the results shown in Fig. 8 (the flow rate at the outlet = 0.90 mm/s). The results indicate that the different viscous SA solutions were well mixed, and a line structure of the mixture was printed when acoustic stimulation was applied to the nozzle (Fig. 9(b)). We demonstrated that the acoustic nozzle effectively mixed viscous bioinks and printing structures in 3D printing. This is the first report on the application of an acoustic micromixer for 3D printing.

In addition, we attempted to print a line structure using a colour gradient. A 0.5 wt% SA solution (red) and a 1.0 wt% SA solution (green) were alternately extruded at 0.90 mm/s from a nozzle with acoustic vibration. A colour gradient was formed under acoustic stimulation with a transition length of approximately 15 mm, whereas it did not form without stimulation, as shown in Fig. 10. The developed nozzle can mix different viscous bioinks while alternately switching between them. Technology for the local arrangement of bioinks is necessary to obtain more functional structures. Lavrentieva et al. reported the formation of a stiffness gradient of a GelMA

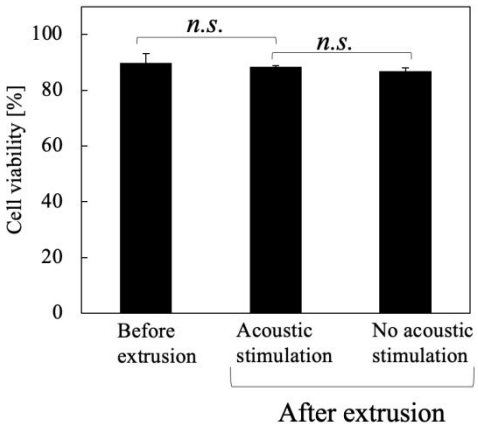

Fig. 11 Effect of acoustic stimulation on cell viability in acoustic micromixer, (n=3, Data: Mean±S.D.)

hydrogel using a static micromixer during bioprinting.[2] However, a long mixing path (>18 mm) was required to mix bioinks, which could cause a delay and requires a complex controlling system. By contrast, our developed nozzle mixes viscous bioinks, such as natural polymers, with a shorter mixing path (5 mm) in 3D printing.

Cell viability test

These cells are typically used for bioprinting studies.[3,49] The effect of the acoustic nozzle on cell viability was also evaluated. The cell suspension in DMEM and a 0.5 wt% SA DMEM solution was mixed with the 0.5 wt% SA DMEM solution without cells in an acoustic micromixer under acoustic stimulation. The cell viability of the cell suspension before extrusion was 89.8 ± 3.3%. The cell viabilities after extrusion were 88.4 ± 0.4% and 86.9 ± 1.0% with and without acoustic stimulation, respectively (Fig. 11). No significant differences were observed between the values ($p > 0.05$). This result showed that the acoustic device did not affect cell viability. Controlling cell density during bioprinting is crucial, as it affects the physiological functions of native tissues, such as cell growth and tissue homeostasis.[50,51] In addition, high cell viability after extrusion is important for obtaining a bioink with the desired cell density.[21,52] Hence, this micromixer has high potential for mixing bioinks and cells to control cell density without causing damage.

Photocurable chitosan printing using an acoustic nozzle

Furthermore, we investigated whether this micromixer could be applied to bioinks other than SA solutions. Chitosan is a cationic natural polymer, while SA is an anionic polymer.[53,54] Chitosan has good biofunctionality, including wound healing and antimicrobial activity, and its phenol derivative (Ch-Ph) can be used as a bioink.[33] The Ch-Ph aqueous solutions at 0.5 and 1.0 wt% were mixed in the developed acoustic nozzle at 0.4–6.4 mm/s. Efficient mixing was confirmed up to 1.6 mm/s (Fig. 12(a), 88 ± 0.6%). In addition, a line structure containing a mixture of 0.5 and 1.0 wt% Ch-Ph was printed similarly to the SA bioink (Fig. 12(b)). This result indicates that the acoustic nozzle can be applied to various types of bioinks.

Limitation and perspective

Our developed nozzle, while effective for mixing 0.5 wt% and 1.0 wt% SA solutions, was unable to mix highly viscous SA solutions (>500 mPa·s) under bioprinting conditions. This limitation highlights the need for further advancements to accommodate the wide range of bioink viscosities used in bioprinting, which can vary from 50–1.0×10^5 mPa·s to meet diverse application requirements.[55–57]

To address the mixing of higher viscosity solutions in an acoustic micromixer, utilising advanced microfabrication techniques could enable the creation of smaller holes for trapping bubbles at the micrometre scale.[58] In this study, we used a commercially available 3D printer for nozzle fabrication. Although this printer was inexpensive and could quickly produce microchannels (in less than 10 min), its resolution was limited to 200 µm (submillimeter scale). This limitation affects the size of the holes required to trap bubbles within the nozzle, thereby restricting the strength of the microstream induced by the bubbles. Smaller bubbles generate more prominent streams inside the nozzle, leading to higher mixing efficiency.[27] However, higher frequencies and increased energy for bubble oscillations may damage cells within the bioink. In particular, cavitation occurs under ultrasound conditions[59] and can deform cells. Therefore, detailed investigations must be conducted to balance cell viability and mixing efficiency.

Exploring materials such as glass or metal for nozzle fabrication can reduce vibration damping and improve the transfer of acoustic stimulation from the piezo to the bubbles. These materials may achieve higher mixing efficiency than the acrylic-based resin used in this study. Future designs could include nozzles with a larger number of inlets arranged to optimise the mixing of several types of inks simultaneously.[60]

Engaging experts in microfabrication and materials science to refine nozzle designs and test new materials should accelerate the development of high-performance micromixers.

Conclusions

A bubble-induced acoustic micromixer was used for 3D printing. First, the effects of the bubble design, frequency, and voltage were investigated. After optimisation, the proper arrangement of bubbles was determined for effective mixing. Based on these results, a nozzle was designed, and the mixing performance was evaluated using different viscous bioinks. The nozzle successfully mixed 0.5 and 1.0 wt% SA solutions and other viscous bioinks with high mixing efficiency under printing conditions. The proposed nozzle could mix different viscous bioinks at a higher flow rate than reported passive mixers and with a smaller volume than reported active mixers. Further

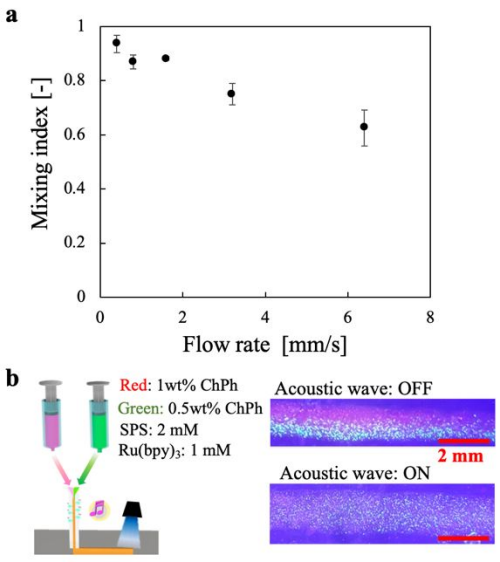

Fig. 12 (a) Mixing performance for 0.5 and 1.0 wt% Ch-Ph aqueous solutions (n = 5, Data: Mean ± SD). (b) Schematic of the 3D printing system and printed line structures of Ch-Ph hydrogel with and without acoustic wave.

design optimisation is needed to mix 2.0 wt% SA solution or more viscous bioinks. Finally, a line structure was printed using the nozzle under acoustic stimulation, demonstrating its ability to mix different viscous bioinks, including SA and Ch-Ph, during the printing process.

In addition, acoustic stimulation did not affect cell viability. This is the first report on the application of an acoustic micromixer for 3D printing. We believe that this technique will expand the applications of 3D printing, particularly in the field of bioprinting.

Author contributions

Mistuyuki Hidaka: Conceptualisation; Investigation; Analysis; Visualisation; Writing—Original Draft; Masaru Kojima: Writing—Review and Editing; Shinji SAKAI: Supervision; Writing—Review & Editing, Project administration.

Conflicts of interest

There are no conflicts to declare

Data availability

Data supporting the findings of this study are available from the corresponding author upon reasonable request.

Acknowledgements

This study was supported by JST SPRING (Grant Number JPMJSP2138) and JSPS KAKENHI (Grant Number 24KJ1594). And, we would like to thank Editage (www.editage.jp) for English language editing.

Notes and references

1. A. I. Shallan, P. Smejkal, M. Corban, R. M. Guijt, M. C. Breadmore*, Anal Chem*, 2014**, 86**, 3124–3130, DOI: 10.1021/ac4041857
2 A. Lavrentieva, T. Fleischhammer, A. Enders, H. Pirmahboub, J. Bahnemann, I. Pepelanova, *Macromol Biosci*, 2020, **20**, 2000107, DOI:10.1002/mabi.202000107.
3 M. A. Heinrich, W. Liu, A. Jimenez, J. Yang, A. Akpek, X. Liu, Q. Pi, X. Mu, N. Hu, R. M. Schiffelers, J. Prakash, J. Xie, Y. S. Zhang, *Small*, 2019, **15**, 1–47, DOI: 10.1002/smll.201805510
4 Z. Gu, J. Fu, H. Lin, Y. He, *Asian J Pharm Sci*, 2020, **15**, 529–557, DOI: 10.1016/j.ajps.2019.11.003
5 J. Nie, Q. Gao, J. Fu, Y. He*, Adv Healthc Mater*, 2020, **9**, 1901773, DOI: 10.1002/adhm.201901773
6 J. K. Placone, A. J. Engler, *Adv Healthc Mater*, 2018, **7**, 1701161 DOI:10.1002/adhm.201701161.
7 X. Li, B. Liu, B. Pei, J. Chen, D. Zhou, J. Peng, X. Zhang, W. Jia, T. Xu, *Chem Rev*, 2020, **120**, 10793–10833, DOI: 10.1021/acs.chemrev.0c00008
8 B. Grigoryan, D. W. Sazer, A. Avila, J. L. Albritton, A. Padhye, A. H. Ta, P. T. Greenfield, D. L. Gibbons, J. S. Miller, *Sci Rep*, 2021, **11**, 1–13, DOI: 10.1038/s41598-021-82102-w
9 S. Ramesh, O. L. A. Harrysson, P. K. Rao, A. Tamayol, D. R. Cormier, Y. Zhang, I. V. Rivero, *Bioprinting*, 2021, **21**, DOI: 10.1016/j.bprint.2020.e00116
10 E. Reina-Romo, S. Mandal, P. Amorim, V. Bloemen, E. Ferraris, L. Geris, *Front Bioeng Biotechnol*, 2021, **9**, 701778 DOI:10.3389/fbioe.2021.701778.
11 A. Schwab, R. Levato, M. D'Este, S. Piluso, D. Eglin, J. Malda, *Chem Rev*, 2020, **120**, 11028–11055, DOI: 10.1021/acs.chemrev.0c00084
12 M. Puertas-Bartolomé, M. K. Włodarczyk-Biegun, A. Del Campo, B. Vázquez-Lasa, J. S. Román, *Polymers (Basel)*, 2020, **12**, 1–17, DOI: 10.3390/polym12091986
13 S. Ishihara, H. Kurosawa and H. Haga, Gels, 2023, **9**, 148DOI:10.3390/gels9020148.
14 J. C. Ashworth, M. Mehr, P. G. Buxton, S. M. Best and R. E. Cameron, J Mater Sci Mater Med, 2018,**29**, 166 DOI:10.1007/s10856-018-6175-9.
15 Y. Zhao, Y. Li, S. Mao, W. Sun, R. Yao, *Biofabrication*, 2015, **7**, 045002, DOI:10.1088/1758-5090/7/4/045002.
16 L. Serex, A. Bertsch, P. Renaud, *Micromachines (Basel)*, 2018, **9**, 86 DOI:10.3390/mi9020086.
17 V. Narayanamurthy, Z. E. Jeroish, K. S. Bhuvaneshwari, P. Bayat, R. Premkumar, F. Samsuri, M. M. Yusoff, *RSC Adv*, 2020, **10**, 11652–11680, DOI: 10.1039/d0ra00263a
18 S. Yin, *Highlights Sci Eng Technol*, 2022, **37**, 208–217, DOI:10.54097/hset.v37i.6076
19 T. J. Ober, D. Foresti, J. A. Lewis, *Proc Natl Acad Sci U S A*, 2015, **112**, 12293–12298, DOI: 10.1073/pnas.1509224112
20 A. M. Golobic, M. D. Durban, S. E. Fisher, M. D. Grapes, J. M. Ortega, C. M. Spadaccini, E. B. Duoss, A. E. Gash, K. T. Sullivan, *Adv Eng Mater*, 2019, **1900147**, 1–7, DOI: 10.1002/adem.201900147
21 K. Nair, M. Gandhi, S. Khalil, K. C. Yan, M. Marcolongo, K. Barbee, W. Sun, *Biotechnol J*, 2009, **4**, 1168–1177, DOI: 10.1002/biot.200900004
22 K. Sritharan, C. J. Strobl, M. F. Schneider, A. Wixforth, Z. Guttenberg, *Appl Phys Lett*, 2006, **88**, 1–3, DOI: 10.1063/1.2171482
23 Z. Chen, P. Liu, X. Zhao, L. Huang, Y. Xiao, Y. Zhang, J. Zhang, N. Hao, *Appl Mater Today*, 2021, **25**, 101239, DOI: 10.1016/j.apmt.2021.101239
24 M. Dao, S. Suresh, T. J. Huang, P. Li, Z. Mao, Z. Peng, L. Zhou, Y. Chen, P. H. Huang, C. I. Truica, J. J. Drabick, W. S. El-Deiry, *Proc Natl Acad Sci U S A*, 2015, **112**, 4970–4975, DOI: 10.1073/pnas.1504484112
25 A. J. Conde, I. Keraite, A. E. Ongaro, M. Kersaudy-Kerhoas, *Lab Chip*, 2020, **20**, 741–748, DOI: 10.1039/c9lc01130g
26 Y. Sriphutkiat, S. Kasetsirikul, D. Ketpun, Y. Zhou, X. Wang, *Sci Rep*, 2019, **9,** 17774, DOI: 10.1038/s41598-019-54330-8
27 D. Ahmed, X. Mao, J. Shi, B. K. Juluri, T. J. Huang, *Lab Chip*, 2009, **9**, 2738–2741, DOI: 10.1039/b903687c
28 Q. Tang, F. Liang, L. Huang, P. Zhao, W. Wang, *Biomed Microdevices*, 2020, **22**, 13 DOI:10.1007/s10544-020-0470-1.
29 Z. Chen, L. Shen, X. Zhao, H. Chen, Y. Xiao, Y. Zhang, X. Yang, J. Zhang, J. Wei, N. Hao, *Appl Mater Today*, 2022**, 26**, 101356, DOI: 10.1016/j.apmt.2021.101356
30 N. Hao, P. Liu, H. Bachman, Z. Pei, P. Zhang, J. Rufo, Z. Wang, S. Zhao, T. J. Huang, *ACS Nano*, 2020, **14**, 6150–6163, DOI: 10.1021/acsnano.0c02145
31 S. J. Song, J. Choi, Y. D. Park, S. Hong, J. J. Lee, C. B. Ahn, H. Choi, K. Sun, *Artif Organs*, 2011, **35**, 1132–1136, DOI: 10.1111/j.1525-1594.2011.01377.x
32 H. Xu, C. Han, S. Liu, X. Hao, Y. Rao, Z. Gong, Z. Sun, *Ionics (Kiel)*, 2020, **26**, 6371–6378, DOI: 10.1007/s11581-020-03773-5

33 M. Hidaka, M. Kojima, M. Nakahata, S. Sakai, *Polymers (Basel),* 2021, **13**, 1382, DOI:10.3390/polym13091382.
34 A. B. Khoshfetrat, M. Khanmohammadi, S. Sakai, M. Taya, *Int J Biol Macromol*, 2016, **92**, 892–899, DOI: 10.1016/j.carbpol.2014.05.010
35 M. R. Rasouli, M. Tabrizian, *Lab Chip*, 2019, **19,** 3316–3325, DOI: 10.1039/c9lc00637k
36 Hiratsuka Laboratory, http://www.jaist.ac.jp/ms/labs/hiratsuka/index.php/動きをトレース (accessed September 2023)
37 G. Cai, L. Xue, H. Zhang, J. Lin, *Micromachines (Basel)*, 2017, **8**, DOI: 10.3390/mi8090274
38 W. Strober, *Curr Protoc Immunol*, 2015, **111**, A3.B.1–A3.B.3., DOI: 10.1002/0471142735.ima03bs111
39 K. Okita, Y. Matsumoto, S. Takagi, *J Fluid Sci Technol,* 2007, **72**, 885–892, DOI: 10.1299/jfst.3.116
40 P. Del Gaudio, P. Colombo, G. Colombo, P. Russo, F. Sonvico, *Int J Pharm*, 2005, **302**, 1–9, DOI: 10.1016/j.ijpharm.2005.05.041
41 S. Sakai, H. Ohi, T. Hotta, H. Kamei, M. Taya, *Biopolymers*, 2005, **302**, 1–9, DOI:10.1002/bip.23080.
42 X. Chen, Y. Tian, *J Chem Technol Biotechnol*, 2020, **95**, 806–812, DOI: 10.1002/jctb.6270
43 Y. L. Y. C. C. Wu, *Biomedical Microdevices,* 2007, **9**, 215–221, DOI: 10.1007/s10544-006-9023-5
44 V. Hessel, H. Löwe, F. Schönfeld, *Chem Eng Sci*, 2005, **60**, 2479–2501, DOI: 10.1016/j.ces.2004.11.033
45 H. Kim, K. Min, K. Inoue, D. J. Im, D. P. Kim., J. Yoshida, *Microfluidics*, 2016, **352**, 6286, DOI: 10.1126/science.aaf1389
46 J. M. Ortega, M. Golobic, J. D. Sain, J. M. Lenhardt, A. S. Wu, S. E. Fisher, L. X. Perez Perez, A. W. Jaycox, J. E. Smay, E. B. Duoss, T. S. Wilson, *Adv Mater Technol*, 2019, **4**, 1800717, DOI:10.1002/admt.201800717.
47 A. Munaz, H. Kamble, M. J. A. Shiddiky, N. T. Nguyen, *RSC Adv*, 2017, 7, 52465–52474, DOI: 10.1039/c7ra08073e
48 A. K. Miri, I. Mirzaee, S. Hassan, S. Mesbah Oskui, D. Nieto, A. Khademhosseini, Y. S. Zhang, *Lab Chip*, 2019, **19**, 2019–2037, DOI: 10.1016/j.biomaterials.2018.08.006
49 S. Tasoglu, U. Demirci, *Trends Biotechnol*, 2013, **31**, 10–19, DOI: 10.1016/j.tibtech.2012.10.005
50 B. Figueroa, F. X. Xu, R. Hu, S. Men, D. Fu, *J Phys Chem B*, 2022, **126**, 7595–7603, DOI: 10.1021/acs.jpcb.2c04355
51 V. C. Hecht, L. B. Sullivan, R. J. Kimmerling, D. H. Kim, A. M. Hosios, M. A. Stockslager, M. M. Stevens, J. H. Kang, D. Wirtz, M. G.er Heiden, S. R. Manalis, *J Cell Biol*, 2016, **212**, 439–447, DOI: 10.1083/jcb.201506118
52 A. Malekpour, X. Chen, *J Funct Biomater*, 2022, **13**, 40, DOI: 10.3390/jfb13020040
53 F. Croisier, C. *Jérôme, Eur Polym J*, 2013, **49**, 780–792, DOI: 10.1016/j.eurpolymj.2012.12.009
54 B. Tian, Y. Liu, *Polym Adv Technol*, 2020, **31**, 2408–2421, DOI: 10.1002/pat.5010
55 S. Sakai, K. Mochizuki, Y. Qu, M. Mail, M. Nakahata, M. Taya, Biofabrication, 2018, **10**, 045007, DOI:10.1088/1758-5090/aadc9e.
56 F. E. Montero, R. A. Rezende, J. V. L. Silva, M. A. Sabino, *Biomacromolecules*, 2019, **20**, 1975–1988, DOI: 10.3389/fmech.2019.00056
57 S. Chawla, S. Midha, A. Sharma, S. Ghosh, *Adv Healthc Mater*, 2018, 7, e1701204, DOI: 10.1002/adhm.201701204
58 D. Deng, L. Zeng, W. Sun, *Int J Heat Mass Transf*, 2021, **175**, 121332, DOI: 10.1016/j.ijheatmasstransfer.2021.121332
59 S. Surdo, M. A. Geven, R. Donno, A. Diaspro, N. Tirelli, M. Duocastella, presented in part at Eurosensors 2018 Conference, Graz, Austria, September, 2018. DOI: 10.3390/proceedings2130942
60 J. O. Hardin, T. J. Ober, A. D. Valentine, J. A. Lewis, *Adv Mater*, 2015, **27**, 3279–3284, DOI: 10.1002/adma.201500222

Data availability

Data supporting the findings of this study are available from the corresponding author upon reasonable request.